Pulsed Laser Deposition of Material

Submitted by
Syed Iftikhar Hussain
2005-MPhil-Phy-01

Supervised by
Dr. Khurram Siraj

Department of Physics
Faculty of Natural Sciences, Humanities, & Islamic Studies
University of Engineering and Technology, Lahore-Pakistan
2009

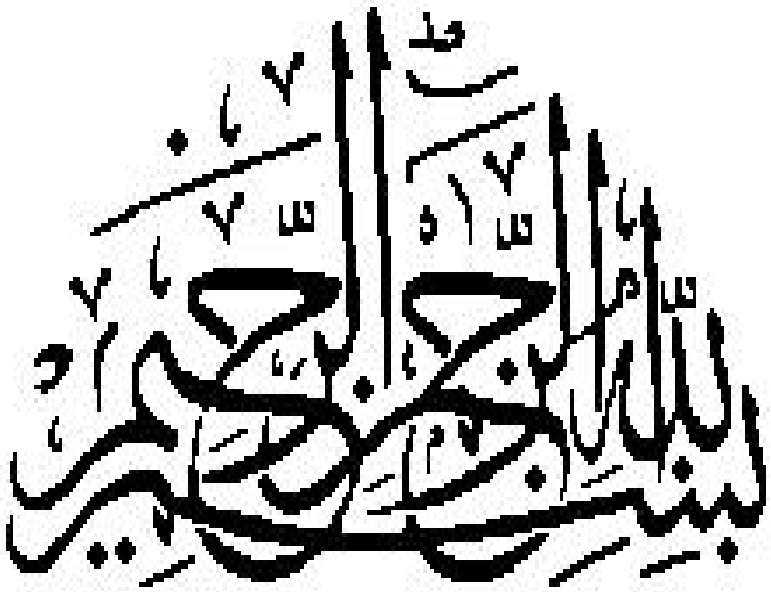

IN THE NAME OF ALLAH, THE MOST MERCIFUL, THE MOST BENEFICIENT

ACKNOWLEDGEMENT

The whole praise to **ALLAH**, the Sovereign power, The creator of universe, Who gave us knowledge, Who made us the super creature, Blessed us with knowledge and enables me to accomplish this task.

All respects are for **HOLY PROPHET MUHAMMAD** (Sallallaho-Alaihe-Wasallam), who is forever a source of knowledge and guidance for whole mankind.

I express my profound gratitude to **Prof. Dr. Muhammad Khaleeq-ur-Rahman** Chairman Department of Physics, UET Lahore, for his personal interest, tremendous cooperation, and keen interest in my research work, valuable suggestions and continuous encouragement during the progress of research

Appreciation is offered to my supervisor **Dr. Khurram Siraj,** Assistant Professor, Department of Physics U.E.T Lahore, for his inspiring guidance, keen interest and continuous encouragement during the completion of my research work.

I extend my gratitude to my all other respected teachers; Dr. Shahid Rafique, Mr. Khurshid Bhatti, and Mr. Anwar Latif. I also want to say thanks to Mrs. Safia Anjum, Mr. Hamid Latif and Mr. Arslan Usman Phd scholar in Department of Physics U.E.T Lahore. At all there sincere wishes and friendly behavior make me able to complete this project.

I would like to express my deep wishes and acknowledgement to my friends Mr. Khalid Javeed, Miss Afsheen Samuel and Mr. Monas Shahzad, whose co-operation, wishes and moral support are always with me. My best regards to my parents, brother, and sisters, for their love, encouragement and prayers that played a very important role in the completion of the project.

At the end, I am once again extremely thankful to Almighty Allah for His continuous blessing on me without which I was unable to complete this research and thesis.

Syed Iftikhar Hussain

LIST OF FIGURES

LIST OF TABLES

CONTENTS

ABSTRACT

The objectives of this work are to deposit and analyze the thin film of Al-doped CdO using Pulsed Laser Deposition (PLD) technique on the Silicon (111) substrate at different growth temperatures. For this purpose, KrF Excimer laser having wavelength 248nm, pulse energy 50mJ, repetition rate 20 Hz is employed to ablate the target. This ablated material is deposited on Silicon substrate, which is placed at a distance of 50mm from the target. The whole experiment is performed in vacuum (10^{-5} torr). The effect of deposition temperature on structural, optical and magnetic properties of the deposited film is studied. The deposited thin film is characterized by using XRD, Photo Ellipsometer and VSM. The surface morphology is also studied by SEM. It is observed that that films grown at room temperature shows preferential growth along (111) direction while at high temperature, it shows the preferential growth along the (200) direction. These films show high Absorptivity and low reflectivity in IR range. The optical band gap energy is shifted to lower energy at high temperature. The obtained values are from 2.8 eV to 2.6 eV. The films also show strong magnetic behavior deposited at high temperature. SEM micrographs show that the uniformity of the deposited thin film is increasing with increase of deposition temperature.

Chapter 1

INTRODUCTION & LITERATURE REVIEW

1.1 Introduction

The invention of laser in 1960 has had a huge impact on many branches of science but also on everyday life. Just 20 years ago, few people had heard anything of CD and DVD players, laser pointers, bar-code readers, or broadband Internet networks—things that we now take for decided. Lasers have become so common that most of us are unaware of the original meaning of the word itself and what actually makes laser such a versatile tool. ”Laser” is an acronym for Light Amplification by Stimulated Emission of Radiation. These words mean that when a material having a suitable energy-level scheme is enclosed in a resonating cavity, the radiation incident on it is coherently amplified by an induced interaction process. The output radiation of a laser has several interesting properties that differentiate it from conventional light beams [1].

Laser beams are monochromatic, coherent, and bright, and typically they have a Gaussian transverse intensity distribution. Furthermore, the beam is highly directional, and it can be focused to a spot whose size is of the order of the laser wavelength. This makes it possible to obtain high energy or power densities in a small volume, which are necessary requirements for efficient processing of materials. In particular, by using short laser pulses with a duration ranging from nanoseconds to only a few femtoseconds and focusing them into a μm^2-sized spot, the power density can be $10^5 - 10^{13}$ W/cm^2. Such values are sufficient for melting and vaporizing most materials, which has made high-power lasers attractive alternatives in drilling, welding, and cutting applications [2].

Melting and vaporization are two examples that how laser beams can interact with materials. If the energy density of the applied laser pulses, fluence (J/cm^2), exceeds a certain material-dependent threshold value, the absorption of the laser-beam energy leads to an ejection of particles from a thin surface layer. This interaction process is called ablation, and the whole technique to remove material in a layer-by-layer fashion is known

as laser ablation [3]. At the moment, the most actively studied application areas of laser ablation include eye surgery and surgery in general, micro machining in engineering and in biology, micro- and nano structuring and accurate lithographic patterning of glass and thin films, conservation of old paintings and sculptures, cleaning of surfaces for component fabrication, synthesis of novel materials such as carbon nano tubes and deposition of thin films of different materials [5].

The preparation of thin films using laser ablation is referred to as pulsed laser deposition (PLD). In PLD, the emitted particles are collected on the surface of a substrate, and after a few hundreds or thousands of laser pulses, a thin film with a thickness of the order of a hundred nanometers is formed. A proper film growth requires that the ablation process takes place in a vacuum chamber where the emitted particle jet can freely expand or where its velocity distribution can be shaped in a controlled way. The main advantage of PLD over conventional techniques to prepare thin films is that the material is stoichiometrically transferred from the target to the substrate. In addition, the technique can be applied to a wide variety of materials—metals, insulators, superconductors, polymers, bones and teeth, and even soft biomaterials such as living cells and proteins—and it is possible to use background gases, e.g., O_2 with oxide materials, during the deposition process [4]. Pulsed laser deposition is particularly attractive in the case of multi-component materials that are difficult to process into thin-film form by other methods. Examples of these materials include ceramic high-temperature superconductors [6].

1.2 Interaction of laser pulses with matter

The interaction of laser pulses with matter can be divided into three different regimes by their timescales. In the femtosecond regime, the absorbed electromagnetic energy of a laser pulse is immediately converted to different excitations of the electron distribution such as plasmons, excitons, electron–hole pairs (in semiconductors), and unbound electrons (in metals). These *electronic processes* are considered the most important interaction mechanisms for the shortest, sub-picosecond laser pulses [7]. Due to the very short timescale, the ablation of particles in the femtosecond PLD can be considered a

direct solid–vapor or solid–plasma transition. The power density can be high enough to cause even dielectric breakdown and multiphoton or avalanche electronic ionization in the material. Ultrafast laser pulses have generally a good ablation efficiency, and the threshold fluence can be many times lower than in the case of, e.g., nanosecond pulses. In addition, since the pulses are too short to couple the electronic energy to the crystal lattice, heat conduction is insignificant and ablation occurs practically without damaging the target [8].

In the case of picosecond and nanosecond laser pulses, the emission of particles is controlled by the conduction and diffusion of the absorbed energy in the lattice. Now the pulses are sufficiently long that the energy of the electronic excitations is transferred to the ions in the crystal lattice via electron–phonon coupling within a few picoseconds. As a result, either the lattice is heated or the interaction leads to the evolution of defects and gradual decomposition of the target surface [9]. If the absorption depth of the material, $1/\alpha$, where α is the absorption coefficient,is larger than the thermal diffusion length, the target surface will be heated to the thickness of $1/\alpha$ independent of the pulse duration. This is the case for many ceramics ablated with picosecond pulses, and it generally results in a significant removal of matter at low fluences. The situation is reversed for metals, for which it typically holds that the absorption depth is much smaller (≈ 10 nm) than the thermal diffusion length: all of the laser-pulse energy is deposited in a thin surface layer and then transported to a volume whose depth is of the order of one diffusion length. This depth is proportional to the square root of the laser-pulse duration. As a result, melting and vaporization take place inside the target and material starts to boil off into the vacuum [10].

In nanosecond PLD, which is the case when using Excimer or *Q*-switched Nd lasers, the situation presented above is complicated by the ionization of the evaporated particle layer. Again, the transfer of energy to the lattice occurs within the picosecond timescale but now there is enough time such that a large part of the target material heats up to temperatures above its melting and boiling points. In the case of metals, the long pulse duration creates a large layer of molten material, from which the evaporation of particles

takes place. The target surface starts to vaporize after approximately 100 ps, and the material under the evaporated cloud is effectively screened from the rest of the laser pulse. Thus, the particle cloud absorbs a significant part of the incoming laser pulse. The process is schematically illustrated in figure 1.1 [10].

The laser-pulse energy is finally converted to the kinetic energy of the emitted particles. The term "sputtering" is used here to distinguish the different emission—or ablation—mechanisms from each other. In *collisional sputtering*, the conservation laws for energy and momentum directly give the maximum transfer of energy from the projectile beam to the target. In the case of photons, however, only indirect collisional effects are of importance: the ions in a plasma plume can interact with the laser beam and, as a result, can be scattered towards the target [4]. In *thermal sputtering*, the particles are evaporated from a heated, partly molten target surface. As mentioned in the previous paragraph, this mechanism is the dominant one when depositing films of metal targets with nanosecond pulses. For short laser pulses, the primary mechanism responsible for the observed non-thermodynamical yield of particles is *electronic sputtering*. Different electronic processes were presented at the beginning of this section, and all of them have the common feature of inducing some form of ionizations or excitations. Electronic processes are also considered the main reason for the ejection of particles when ablating semiconductors or insulators with nanosecond pulses [11].

The laser fluence has to be higher than a certain threshold value such that stoichiometric ablation takes place. The fluence can be increased either by increasing the pulse energy or by shrinking the dimensions of the laser spot on the target. However, too tight a focusing of the beam can result in a low removal rate of matter, the ejection of droplets or large particulates from the target, or the formation of cone like structures in the surface, possibly enriched with respect to some element. Thus, the surface modification of the ablated targets as a function of the fluence and the pulse duration has attracted much research interest [10, 11].

The threshold value for the fluence has been determined for several different materials, and its dependence on the wavelength, the pulse duration, and the beam radius have been widely studied [12]. For noble and transition metals, the threshold value is of the order of 1−2 J/cm^2 ,for refractory metals such as Mo, Re, and W it is higher than 10 J/cm^2, and for ceramics such as YBCO approximately 1 J/cm^2. Generally, the larger the fluence, the fewer droplets or off-stoichiometric particulates are emitted but too high a fluence may lead to the sputtering of unwanted debris from the target. In addition, the shorter the pulse, the higher its spatial and temporal uniformity should be to ensure homogeneous ablation.

In PLD, lasers operating at UV wavelengths are commonly used since at short wavelengths the reflectivity of most materials, in particular that of metals, is much lower than in the IR regime. This promotes the absorption of the laser light and increases the ablation efficiency. Since also the absorption coefficient is large in the UV region, the beam energy is absorbed in a thin surface layer, which further intensifies the ablation process.

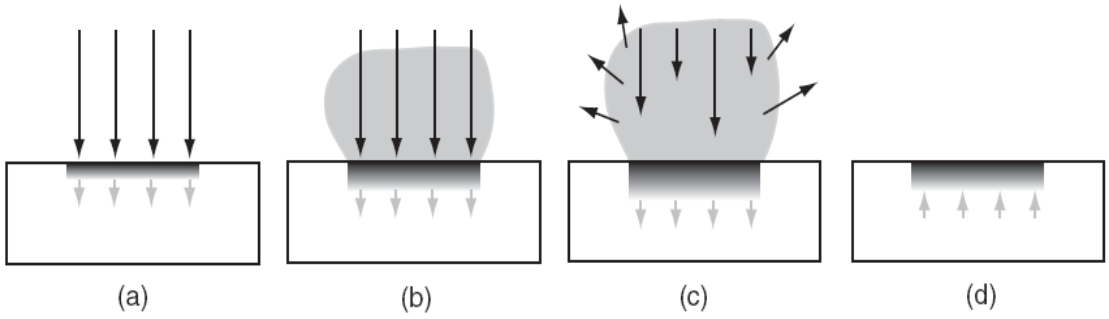

Figure 1.1: Schematic illustration of the ablation process in the case of nanosecond PLD.(a) Initial absorption of laser radiation (black arrows) and melting of the target material (grey arrows indicate the motion of the solid–liquid interface). (b) The melt front propagates into the solid and the evaporation of particles begins. (c) The plume absorbs the rest of the laser radiation and fully ionized plasma is formed. (d) The melt front starts to recede after the laser pulse and the target is re-solidified [4].

1.3 Plume formation and propagation

The material evaporated or otherwise ejected from the target is hot and partially ionized. In the nanosecond regime, this particle cloud absorbs further energy from the laser pulse that has initiated it, becomes more and more ionized, and finally fully ionized plasma develops. The particles in the high-pressure plasma collide with each other until the bubble reaches thermal equilibrium at a distance of ≈ 50 μm from the target, in the so-called Knudsen layer [5]. After this point, the particles can be described by the Maxwell–Boltzmann statistics, and the plasma *plume* starts to expand like a pulsed jet from a nozzle at supersonic velocities in the direction of the target normal. Typically, the spreading of the forward-peaked plume is modelled by a $\cos^n \theta$ law where n (not necessarily an integer) ranges from 1 to 10 depending on the material and the ablation parameters and θ is the scattering angle [4].

The plume consists of ions, electrons, neutral atoms, particle clusters, and macroscopic particulates originating from the target or resulting from condensation and nucleation of particles in the supersaturated vapor. The emitted light and the color of the plume are caused by fluorescence and recombination processes in the plasma. Although atomic transitions typically have lifetimes of the order of a few nanoseconds, collisions can re-excite atoms such that the characteristic emission lines are observed even microseconds after the laser pulse [4].

As the plume expands, it rapidly evolves both in space and in time: the different species in the plume have different kinetic energies and their energy distributions will change as a result of interactions with other particles in the plasma. For example, the strong Coulomb force between electrons and ions prevents the electrons from escaping from the dense plume. Thus, they are decelerated with respect to neutral particles although they are light and have a high mobility [5]. The ions, on the contrary, are accelerated to higher velocities than the neutral species in the plasma. The electron temperature varies more slowly as a function of θ than the ion temperature, which, moreover, is peaked along the target normal. Typical values for the temperatures in an expanding plasma are 0.1−0.5 eV for electrons, 1−100 eV for ions, and a few eV for neutral particles [12, 13].

In an ambient gas, the plume behaves in a different way than in vacuum. In vacuum, the plume can be considered to expand adiabatically albeit, due to the high density of the plasma, the expansion is not completely unidirectional but backward velocity components appear as well. The molecules of the background gas, on the other hand, scatter, attenuate, and finally thermalize the plume. In addition, reactive scattering, e.g., with O_2 can produce clusters and molecules which are essential for the proper stoichiometry of the growing film. As the pressure of the background gas increases, at first the fluorescence becomes more prominent. Then, the plume boundary sharpens and the plume itself becomes slower and better confined. At high pressures, a shock front is formed as the plume compresses the background gas. This results in an audible shock wave with a clicking sound (at atmospheric pressures) and, finally, the plume diffuses into the ambient gas [15].

The fluence has a significant effect on the shape, size, and visibility of the plume. As the fluence increases, the visible part of the plume becomes longer due to the increasing energy of the ablated species but the angular distribution is not considerably altered. At high fluences, the plume can tilt away from the target normal, probably due to the formation of cones, cracks, craters, or columnar structures on the target surface. A similar tilting effect is observed when the laser beam has a non-uniform intensity distribution or the laser spot size on the target is reduced too much. Decreasing the spot size but keeping the fluence constant results in an inefficient removal of matter and widening and shortening of the plume. In addition, the angular distribution of the plume in the substrate plane may change when the target–substrate distance is increased, in particular, when depositing the films in the presence of some background gas [4].

1.4 Film condensation

1.4.1 Different growth modes

The nucleation of a film is basically determined by the equilibrium between the vapor and solid phases of the material ejected from the target. Every compound has a tabulated, temperature-dependent equilibrium vapor pressure, and if the real vapor pressure of the

arriving particle jet is larger than this equilibrium value, it is energetically favorable for the vapor to condense onto the substrate. The actual film growth can be further divided into four different modes depending on how the atoms arrange themselves on the substrate: three-dimensional growth of particle islands, two-dimensional formation of full monolayers, growth of islands on top of monolayers, and the so-called step-flow growth where the film follows the step–terrace structures of the substrate [16].

In the three-dimensional growth mode, the particles incident on the substrate surface form clusters which start to grow in size such that the resulting film finally consists of large but separate islands of atoms. The atomic processes connected to the nucleation and disintegration of clusters are presented in figure 1.2. Thermodynamically, all these processes change the total free energy of the film–substrate–vapor system. The cluster will grow if the derivative of the free energy with respect to the number of atoms in it is negative. This condition is met beyond a certain critical radius which is a function of temperature and supersaturation of the incoming vapor. The formation of a stable cluster can also be described in terms of surface energies. If the sum of the surface energies in the cluster–vapor and substrate–cluster interfaces is larger than the corresponding surface energy for the substrate–vapor interface, the film will grow three-dimensionally since the area-to-volume ratio of a cluster is now smaller than that of planar structures [4]. The island growth can be promoted by decreasing the temperature and increasing the supersaturation, i.e., the deposition rate. On the other hand, if the supersaturation is very high during a single burst of particles followed by a longer period without a particle flux, the clusters will have time to evolve into full monolayers due to the high mobility of the atoms [18].

If the above-mentioned inequality for the surface energies is not satisfied, the film grows as full monolayers. This growth mode can also be considered to involve the formation of clusters but their radius is small and they are only one-monolayer thick. Two-dimensional growth takes place typically at high temperatures and at reasonably low supersaturations (deposition rates are not too high), and generally this layer-by-layer-type film growth results in epitaxial films with an atomically smooth surface. However, large periods

between successive laser pulses can somewhat complicate the situation: the size of a critical cluster can grow and the subcritical clusters may adhere into larger clusters promoting three-dimensional film growth [4, 19].

The third common growth mode is that after a few monolayers islands start to form and increase in size. This effect, mainly resulting from increased stress with increasing layer thickness, is due to a non-perfect lattice match between the film and the substrate. Island formation on top of monolayers has been observed, in particular, when depositing films of elemental metals [4].

The fourth way how the film can grow is the step-flow growth or, more generally, heterogeneous nucleation. For instance, atomic steps, point defects, and dislocations in the substrate provide additional nucleation sites for the incoming particles. Again, the onset of this growth mode depends on the various process parameters and on the film thickness: the temperature has to be high such that the island growth is suppressed and the deposition rate should be high such that the particles would not condense on a single monolayer but follow the seeds in the substrate. However, the thicker the film, the more probable it is that transition to the three-dimensional growth mode occurs [16].

To obtain high-quality films in terms of their crystallinity and surface smoothness, the film should grow two-dimensionally, as full monolayers. A high substrate temperature, a reasonably large supersaturation of the particle plume and a properly lattice-matched and chemically inert substrate material are necessary prerequirements for this type of film growth. In addition, the sticking coefficient of the film to the substrate should be large and the thermal expansion coefficients of the film and the substrate should not differ too much from each other. The background gas has a large effect on re-sputtering from the growing film but it can also prevent chemical reactions with, e.g., the residual oxygen in the deposition chamber. To meet many of the criteria mentioned above, Blank *et al.* have developed an interval deposition technique: one monolayer is quickly deposited using a high supersaturation followed by a break long enough such that the film has time to reorganize and grow in a layer-by-layer fashion. This guarantees a high nucleation

probability during the short deposition interval but also decreases the size of three-dimensional islands and the probability for the particles to nucleate into them during the pauses [17].

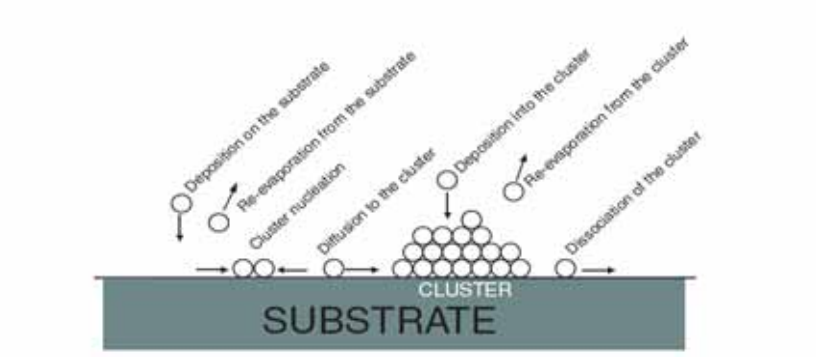

Figure 1.2: Different atomic processes in the nucleation of three-dimensional clusters on the substrate [4].

1.4.2 Particulates on the film surface

The number of particulates on the surface is another issue that affects the overall film quality. The particulates can be categorized into small droplets (whose diameters range from a few nanometers to one micrometer) and large, possibly irregularly-shaped outgrowths (diameters up to tens of micrometers). The number density of the particulates depends on the fluence, the number of laser pulses on the target, and on the deposition parameters such as the substrate temperature and the background-gas pressure. The largest particulates are believed to originate directly from the target: breaking of protruding surface features, mechanical disintegration of, e.g., cones, craters, or micro cracks, ejection of large droplets due to thermal shocks, splashing of a molten surface layer, or violent expansion of gas bubbles under a solid layer are typical explanations for their emergence. Droplets, on the other hand, are either re-solidified objects ejected from the target or other species condensed from the supersaturated vapor on the substrate. By adjusting the deposition parameters properly, the particulate density can be minimized but, simultaneously, the number of so-called precipitates can increase. The precipitates are particulates with a stoichiometry totally different from that of the film matrix and they are a sign of good crystallinity: off-stoichiometric areas are excluded from the otherwise perfect film into a separate phase. The enrichment of the particulates or precipitates with

respect to some element is typical for films deposited from metal-alloy targets since elements with a low melting point and a high vapor pressure are evaporated first thus making the target deficient in these components [4].

The particulate density is the highest off the deposition axis but the on-axis particulate density can also be high if the target–substrate distance is too small or the velocity of the species in the plume is too high. A high enough substrate temperature and a moderate background-gas pressure reduce the number of droplets and outgrowths on the film surface; reactive scattering at high pressures may lead to the nucleation and growth of additional particle clusters. The fluence has a complicated influence on the distribution and size of the particulates: the larger the fluence, the larger the particulates are but the smaller their number is on the deposition axis. Furthermore, the pulse repetition rate should be low enough such that the condensed species would have time to form a smooth layer with the correct stoichiometry but too low a rate should be avoided such that chemical reactions would not take place [4]. For example, repetition rates of the order of 1−10 Hz promote the growth of YBCO in the desired orthorhombic high-temperature phase and result in a smooth film surface, whereas in the case of yttrium-iron-garnet films, the repetition rate should be above 20 − 30 Hz to prevent the loss of oxygen from the film matrix [30]. At the moment, there are only a limited number of studies on the effect of the laser-pulse duration on the film quality. Klini *et al.* have deposited ZnO films using nanosecond and femtosecond pulses at 248 nm and concluded that femtosecond PLD produces rougher surfaces with a higher number of small crystallites on the surface than nanosecond PLD [21].

1.5 Literature review

R.K. Gupta et al studied the conductive and optical properties doped cadmium oxide thin films, which they deposited on quartz with a KrF excimer laser. The effect of oxygen pressure on structural, electrical, and optical properties is studied. They observed that at high oxygen pressure, the conductivity and band gap energy is decreasing [22].

R.K. Gupta et al studied the conducting and optical properties tin doped cadmium oxide deposited on quartz substrate using PLD. They observed the effect of deposition temperature on these properties. The films show high transmittance in visible region where as resistivity is deceasing at high temperature [23].

R.K. Gupta et al studied the thin films of indium doped cadmium oxide deposited on quartz substrate using PLD. The observed the effect of deposition temperature and oxygen pressure on structural, optical and electrical properties. At high temperature the transparency of the films increases but there is no effect of pressure on this property. They observed that at high deposition temperature and pressure, electrical conductivity is increasing [24].

B. Saha et al observed the thin film of Cadmium oxide with different percentages of aluminum doping deposited by RF sputtering technique. They deposited thin films on glass and silicon substrates having different percentages of aluminum at room temperature. They observed that conductivity and optical band gap is increasing with the increase of doping percentage and then starts decreasing [25].

J. Santos-Cruz etal deposited thin film of un-doped cadmium oxide by sol gel method. They observed the effect of annealing temperature on structural, optical and electrical properties of the deposited film. They observed that, the crystallinity, resistivity and particle size increase with the raise of annealing temperature [26].

Wei-na Miao et al studied an amorphous oxide thin film of molybdenum-doped indium oxide (IMO) deposited by reactive magnetron sputtering at room temperature. The films

formed on glass microscope slides. They observed the effect of oxygen contents on optical and electrical properties [27].

R. Mamazza et al deposited the thin films of cadmium tin oxide on glass substrates by RF sputtering from cadmium oxide (CdO) and tin oxide (SnO_2) targets in an Argon ambient. They deposited thin film at room temperature and observed the effect of annealing temperature on electrical and optical properties. They show that resistivity and band gap energy is increasing with the increase of annealing temperature [28].

W. Beyer et al studied the application of TCO thin films of Aluminum doped zinc oxide and fluorine doped tin oxides thin films. They studied the opto-electrical properties for solar cells application [29].

R. Maity et al studied the Aluminum doped cadmium oxide thin films The films were deposited on glass substrate by sol gel method. They observed the effect of concentration of cadmium acetate dehydrate as precursor on electrical properties of the deposited films. They show that, the conductivity is increasing with the increase of concentration of aluminum [30].

I. Saadeddin et al studied doped SnO_2 thin films prepared by sputtering from two different targets. They observed the mol concentration and post annealing temperature on opto-electrical properties of the deposited films. They shows that, the optical and electrical properties are increasing with increase of concentration and temperature [31].

Sang-Moo Park et al deposited thin films of ZnO on quartz substrate using PLD technique. They observed the effect of temperature and pressure on structural, optical and electrical properties of deposited films [32].

C.H. Bhosale et al used spray pyrolysis technique to deposit thin films of cadmium oxide on amorphous and fluorine doped tin oxide glass substrate. They studied the concentration of cadmium solution on the opto- electrical properties of thin films. They

observed that by increase of concentration of cadmium in solution, the resistivity and band gap energy is decreasing [33].

R.K. Gupta et al studied the electrical and optical properties of thin films of molybdenum doped indium oxide deposited on quartz substrate using PLD technique. They observed the effect of growth temperature and pressure on structural, optical and electrical behavior of deposited thin films. They show that these properties of thin films are highly effected by deposition temperature and pressure [34].

Lei Zhao et al studied and deposited the thin film of ZnO using PlD by ablating the target of zinc in the presence of oxygen pressure. They observed the effect of temperature on the optical and electrical properties of deposited thin film on glass substrate [35].

D. Kim et al deposited thermo electric thin film of bismuth telluride on silicon substrate by RF sputtering technique. the thermoelectric bismuth telluride thin films were prepared on SiO_2/Si substrates by radio-frequency (RF) magnetron sputtering. They studied the effect of temperature and pressure on structural, optical and electrical behavior of the deposited thin films. They observed that these properties are highly affected by these parameters [36].

L.R. de León-Gutiérrez et al deposited the thin films of tin doped and un-doped cadmium oxide thin films using chemical bath method. They observed that doping of tin in cadmium oxide have great effect on opto-electrical properties of thin films [37].

T.K. Yong etal using PLD technique to deposit thin film of Indium tin oxide on polycarbonate in the presence of oxygen at room temperatue. They observed the effect of oxygen pressure on structural, optical and electrical properties of the deposited thin films. They show that crystallinity, band gap energy and conductivity is increasing with the increase of of oxygen pressure [38].

Walter Wohlmutha et al using sputtering depositing technique to deposit the thin films of Indium tin oxide and cadmium tin oxide on quartz substrate and different temperature. They observed the effect of deposition temperature on electrical, optical, structural, chemical, and etch properties of deposited thin films. They show that these properties are highly dependent on growth temperature of the deposited thin films [39].

E.J.J. Martin et al studied the designing and fabrication of multilayered transparent conducting oxide film to achieve both high conducting and high optical transmittance in the visible spectrum. They observed and studied the effect of deposition temperature on these properties [40].

Chapter 2
EXPERIMENTAL WORK

In this research work thin films of Aluminum doped Cadmium Oxide (Al-doped CdO) is to be grown by PLD technique on Si (111) substrate at different growth temperature. In this chapter details about the materials used, sample preparation, experimental setup and techniques employed are given as follows.

2.1 Target Fabrication

An Al-doped CdO target for PLD was prepared by a standard solid-state reaction method. The raw materials used for preparation of target were powders of Al_2O_3 and CdO. All these oxides have same purity better then 99%. Required amounts of CdO and Al_2O_3 were taken by molecular weight. The target has two atomic weight percent of aluminum. The accurate weighing was done by a micro electrical balance (Ogawa Seiki Co. Ltd Japan). After weighing the required amount, the powder was mixed thoroughly using a fine quality mortar and pestle. The well-ground mixture was heated in air using electric furnace (Ogawa Seiki Co. Ltd Japan) at 850 °C for 10 hours. The powder mixture was then cold pressed at 5 tons load using hydraulic press (Model 3010-2 Apex Construction Ltd UK). The pellets were then sintered at 900 °C for 10 hours.

2.2 Substrate

P-type single crystal Silicon with purity 99.99% is used as a substrate. Crystal orientation of silicon is (111). Boron was added as an impurity to built p-type silicon. Silicon is physically a dark grey with a bluish tinge and is solid at 298 K. P-type Silicon is a semiconductor. Silicon is used as a substrate in solar cells and other opto-electrical devices. Silicon sample of 1cm by 1cm dimensions and one side polished is mounted on substrate holder for deposition of Al-doped CdO thin film.

2.3 Excimer laser

Excimer lasers are a group of pulsed lasers that incorporate electronic transitions within short-lived molecules. Such lasers are often composed of the combination of the rare-gas

atom (such as Ar, Kr, or Xe) and a halogen atom (Fl, Cl, Br or I).The word Excimer is a contraction of the phrase "excited dimer". Excimer lasers typically emit in the ultraviolet spectral region, although some operate in the visible spectrum. The principal Excimer laser transitions occur in the XeF at 353 nm, XeCl at 308 nm, KrF at 248 nm, ArF at 193 nm, and F_2 at 153nm. Excimer lasers have very high gain thus normally produce a high order multi-mode output. Their high pulse energy and ultraviolet output make them attractive for materials processing application.

The Excimer laser is produced by forming exited-state species of the Excimer molecule in the upper laser level. Since the ground state of these molecules is not stable, it is not possible to produce the upper level by direct pumping from such a ground state. Therefore, indirect pumping is necessary. The laser medium includes noble-gas such as Krypton, and fluorine molecules in the form of F_2. When an electrical discharge or an electron beam is initiated within the medium, the noble-gas atoms are excited and ionized, leaving for example Kr* or Kr^+, and the fluorine molecules are dissociated to produce F atoms. Many of the F atoms rapidly collect a free electron (produced by ionizing the Kr) to form F^- negative ions. The excited Excimer molecules of KrF* in the upper laser level are then produced by collisions between these two species via the following reactions:

$$\mathbf{Kr^+ + F^- \rightarrow KrF^*,} \qquad \mathbf{(2.1)}$$

$$\mathbf{Kr^* + F^* \rightarrow KrF^*} \qquad \mathbf{(2.2)}$$

The KrF* molecules subsequently radiate, leaving them in the ground state of KrF, which immediately dissociates to produce Kr and F atoms. The process then begins again when the next pulse of electrons is produced within the gain medium [41].

The Excimer laser used in the experiment is KrF 248 nm (Ex50, GAM LASER INC, USA). Following are the specification of the laser

Table 2.1: Specification of KrF Excimer Laser

Parameters	Values
Wave length	248 nm
Max. Energy	50mJ
Average Power @100Hz	4 W
Average Power @250Hz	10 W
Average Power @500Hz	20 W
Repetition rate	20Hz-500 Hz
Pulse Length	16-20 ns
Beam Size	9 × 4 mm
Stability	< 2%Standard Deviation
Divergence	0.8 × 1.6 mRad

2.4 Turbo molecular pump

To obtained and maintian high vacuum, a vacuum pump known as turbo molecular pump is used. Its working based on momentum of the gas molecules in a particular direction with continuies collision on a solid surface.It consit on a spinning turbine rotor which strike the gas molecules from inlet of the pump towards the outlet to maintain a vacuum. This pump is a very versatile pump. It can create vacuum from intermediate level to ultra-high vacuum levels [42].

2.5 Vacuum Chamber

Deposition chamber is one of the most crucial components in a PLD system. In our experiment, chamber is made up of stainless steel to avoid the corrosion. Stainless steel is preferred for large systems because of its relatively high strength, ease of welding and machinability. The system consists of vacuum chamber, pumping system, deposition source and monitoring equipments.

In addition, standard ports are required on all vacuum chambers (e.g. pumping ports, gas inlets and pressure gauging and viewing ports). The PLD chamber must have ports for target and substrate holders, laser window and measuring sensors.

There are multitudes of possible geometries to choose the form of chamber, spherical chamber and cylindrical chamber. With regard to chamber it is wise to remember that target must be mounted or demounted frequently and laser window must be kept clean. Thus, access to target and laser window should be as simple as possible.

If the substrate is heated the chamber will be heated and may have to cool externally; in well designed chamber heat will be distributed uniformly over the surface thus minimizing the need of external cooling. Another important thing is that we prefer spherical chamber to keep the pressure balance.

2.6 Diagnostic Techniques

Following diagnostic techniques have been used to observe the structural, optical, magnetic propeties and surface morpholgy of the deposited thin film.

2.6.1 X-ray diffraction (XRD)

X-ray diffraction is a powerful too for studying both x-ray spectra and arrangement of atoms in the crystals. We can study the crystal itself by using a monochromatic x-ray beam to determine not only the spacing of various crystal planes but also the structure of the unit cell. Figure 2.1 shows an incident wave striking the family of planes, the incident rays making an angle θ with the plane. For the single plane, mirror –like reflection occurs for any value of θ. To have a constructive interference in the beam diffracted from the entire family of planes in the direction θ, the rays from the separate planes must reinforce each other. This means that the path difference for rays from adjacent planes must bean integral number of wavelengths or

$$2d\sin\theta = m\lambda \qquad \text{m=1,2,3…..} \qquad \textbf{(2.3)}$$

This relation is called the Bragg's law. The quantity d in this equation (inter-planar spacing) is the perpendicular distance between the planes [43].

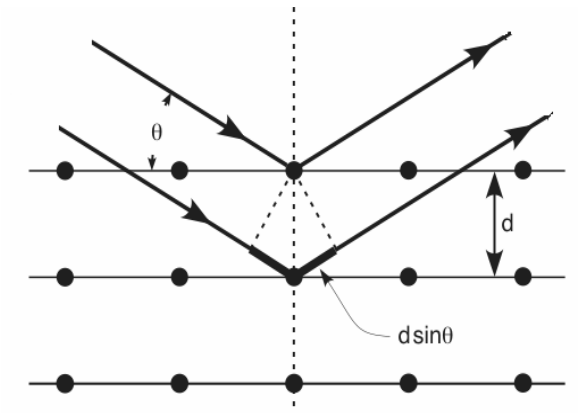

Figure 2.1: An incident beam falls on the set of planes. A strong diffracted beam will be observed if Bragg's law is satisfied [43].

2.6.2 Ellipsometry

Optical measurements are studied by Spectroscopic Ellipsometry (VASETM J.A. Woollam Company). The measurements are made in a suitable wavelength range and in air at room temperature with proper angle of incidence of the light beams on the sample surface.

Ellipsometry is an optical analytical technique which can be used to determine the complex refractive index and thickness of a film material. It works on the difference in reflection coefficient for perpendicular (s-direction) and parallel polarized (p-direction) light. That is, at reflection at a surface the polarization direction of polarized light will change [44]. The change itself is dependent on the optical properties of the material at which the reflection takes place. The calculated values are expressed as Ψ (relative amplitude change) and Δ (relative phase change).

2.6.3 Vibrating sample magnetometer (VSM)

A vibrating sample magnetometer (commonly known as a VSM) vibrates a sample sinusoidally up and down, inducing an electrical signal in a stationary pick-up coil. The signal is proportional to the magnetic moment, as well as to the amplitude and frequency of the vibration. The atomic dipoles align themselves in the direction of external field. A

part of the alignment will be retained in the material after removal of external field. The Hysteresis loop is the relationship between magnetic field strength (H) and magnetic flux density (B). The 'thickness' at the middle of the loop describes the amount of hysteresis, related to the coercivity of the material. Hysteresis loop expected for measuring the magnetization as a function of applied magnetic field, the sample is magnetized to the saturation magnetization M_s by an applied field H. The magnetization reduces to remanent magnetization M_r when the applied field is reduced to zero. A magnetic field equal to the coercive field H_c is needed to switch the magnetization into the opposite direction [45].

2.6.4 Scanning Electron Microscope (SEM)

The scanning electron microscope (SEM) studies the sample surface by scanning it with a high energy beam of electrons in a raster scan pattern. The electrons interact with the atoms of sample and produce signals that give information about the topography of sample's surface [46].

2.6 Experimental procedure

The thin films of Al-doped CdO were deposited on Silicon substrate at 25 °C, 100 °C, 200 °C, 300 °C and 400°C. For this purpose, Pellet of Al-doped CdO was used as a target. P-type, single crystal, polished Silicon (111) was used as a substrate. Dimensions of the substrate were (1 x 1 x 0.2 cm^3). Substrate was mounted on substrate holder which was stationary. Target was mounted on target holder which was rotated by 12V stepper motor. In order to avoid local thermal effects and crater formation, KrF Excimer laser (Ex50, GAM LASER INC, USA) λ = 248 nm with a repetition rate of 20 Hz and a constant voltage mode of 12 kV (pulsed energy 12.5 – 23 mJ) was used for PLD The laser beam was tightly focused by 20 cm UV lens onto Al-doped CdO rotating target at an angle of 45° placed in PLD chamber under vacuum of 10^{-5} torr. As a result, plasma was produced due to material ablation from the target surface. Target was irradiated with 6000 laser shots to deposit thin film of Al-doped CdO. Substrate was placed at a distance of 50 mm. Structural analysis of thin film was done by XRD; optical measurements were made by UV-visible Ellipsometry. The magnetic properties were observed by vibrating

sample magnetometer. The surface morphology of the deposited thin films was studied by SEM. Schematic of the experimental setup used for PLD is show in figure 2.2.

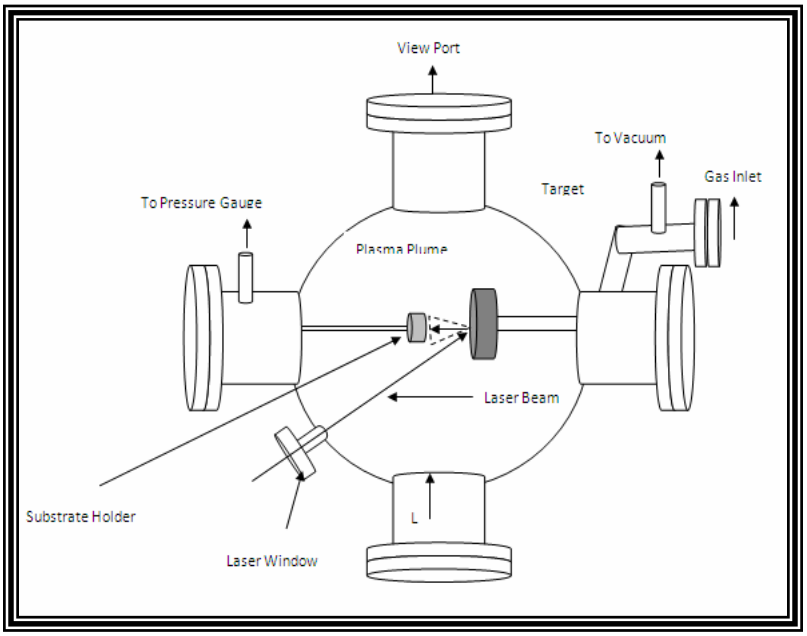

Figure 2.2: A Schematic Diagram of Spherical Vacuum Chamber used in the experiment.

Chapter 3
RESULTS AND DISCUSSION

Aluminum doped Cadmium Oxide (CdO: Al) thin films were deposited on Silicon (Si) substrate at different temperature. The crystal structures of deposited thin films were examined by XRD analysis. The optical and magnetic properties were characterized by photo Ellipsometry and vibrating sample magnetometer. Surface morphology was studied by SEM

3.1 Structural characterization

The structural characterization was done with X-ray Diffractometer (D8 Discover, Bruker, Germany). The diffraction patterns of Al-doped CdO thin films grown under different temperatures are shown in figure 3.1. The films grown at room temperature shows preferential growth along (111) direction, while the films grown at high temperature show preferential growth along the (200) direction. The peaks are in good agreement with JCPDS X-ray file data. The average particle can be determined using Scherrer's formula from the full width half maximum (FWHM) [47].

$$D = \frac{k\lambda}{\beta \cos\theta} \qquad \textbf{(3.1)}$$

Here the constant k is the shape factor ≈ 0.94, λ is the wavelength of the X-rays (1.5406 Å for CuKα), θ is the Bragg's angle, and β is the FWHM. The lattice parameter a is determined by the following expression [47].

$$\frac{1}{d^2} = \frac{h^2 + k^2 + l^2}{a^2} \qquad \textbf{(3.2)}$$

The average value of the lattice parameter a is 4.73 Å. The observed diffraction patterns indicate the polycrystalline nature of CdO with cubic structure. No extra peaks due to addition of Aluminum in cadmium oxide films were observed which indicates the absence of an impurity phase in the films. The structural parameters were calculated and the results are given in Tables (3.1).

Table 3.1: XRD data of Al-doped CdO films grown at (a) 25 °C, (b) 100 °C, (c) 200 °C (d) 300 °C, (e) 400 °C.

Samples no.	**2θ of (200) plane**	**d spacing(A^o)**	**Δ2θ**	**FWHM in Degree β of (200) plane**	**Particle size D (nm)**
1	38.02	2.36484	0.58	0.29	27.076
2	38.015	2.36512	0.44	0.22	35.691
3	38.024	2.36505	0.39	0.198	39.656
4	38.0245	2.36499	0.33	0.167	47.017
5	38.025	2.36503	0.29	0.146	53.780

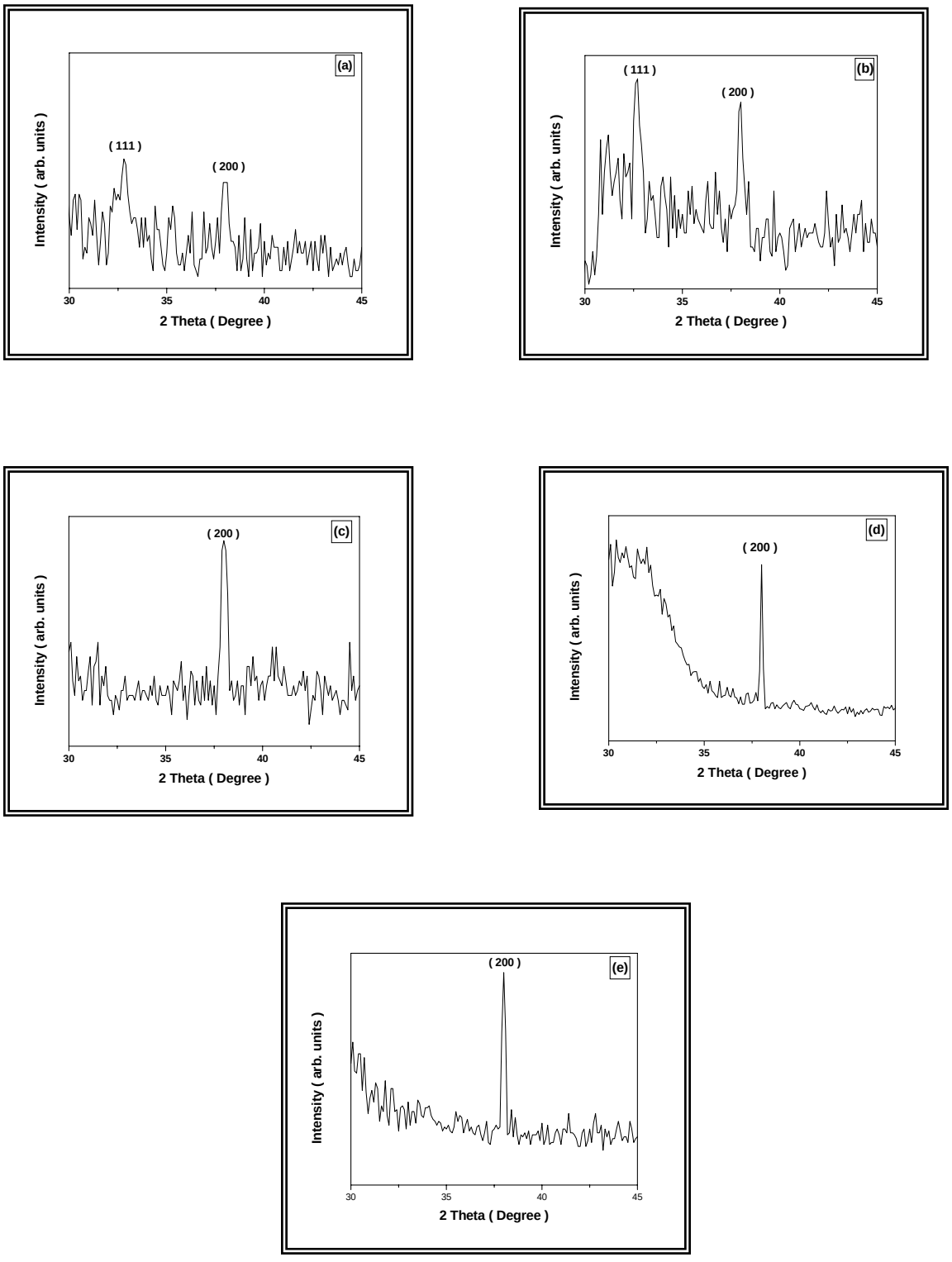

Figure 3.1: XRD patterns of Al-doped CdO films grown at (a) 25 °C , (b) 100°C , (c) 200 °C (d) 300 °C , (e) 400 °C

3.2 Optical characterization

The optical properties of Al-doped CdO thin films were characterized by Ellipsometer. The optical constants are use to define the interaction of light with material. The complex refractive index of the optical constant of a material is represented by [48]

$$N = n + ik \tag{3.3}$$

The real part or refractive index n describes the phase velocity of light in the medium. The wavelength dependence of refractive index plotted in figure 3.2. It is observed that refractive index of all deposited thin films first increases from 200 nm to 400 nm, then remain same from 400nm 1000 nm. But due to increase of the growth temperature it starts decreasing from room temperature to higher one. All deposited thin films show the same behavior at different temperature.

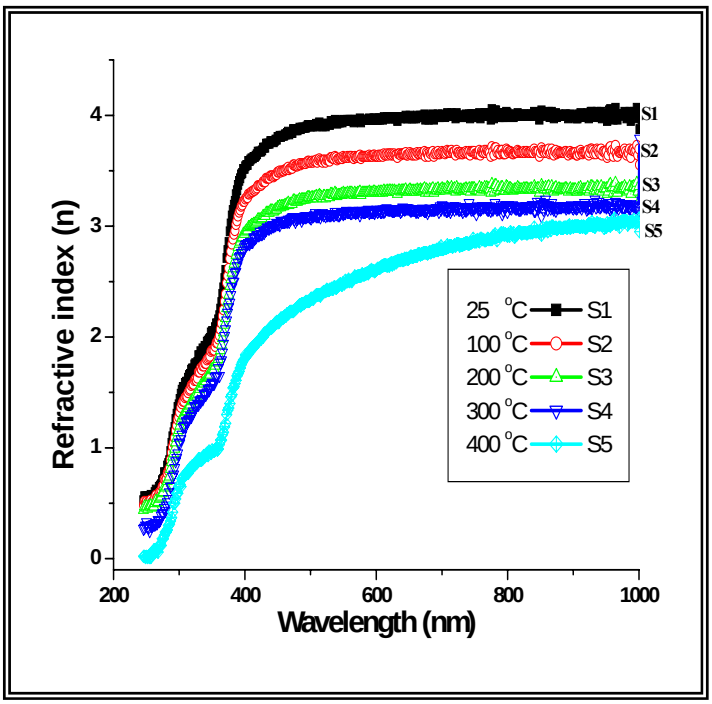

Figure 3.2: Refractive index of Al-doped CdO thin film deposited at different temperature.

The imaginary part or extinction coefficient **k** of complex refractive index defines a measure of the extent by which the intensity of a beam of light is reduced by passing through the material. The extinction coefficients of the deposited in thin films at different growth temperature is shown in the figure 3.3. Results shows that from 200 nm to 380 nm it is increasing and then starts decreasing from 380 nm to 1000 nm. All the deposited films show same behavior. It can also be observed that extinction coefficient of the deposited thin film is temperature dependent which is increasing from room temperature to the higher one.

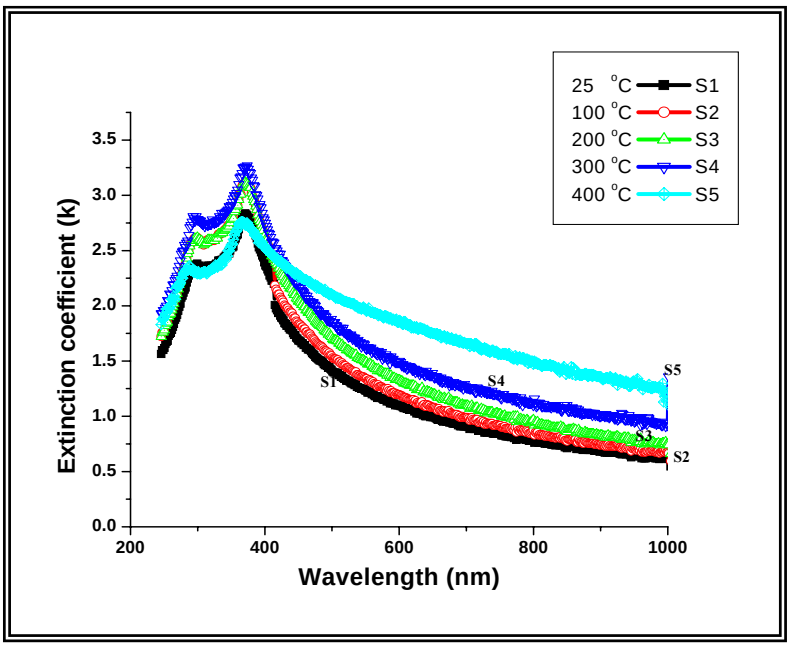

Figure 3.3: Extinction coefficient of Al-doped CdO thin film deposited at different temperature.

In optical measurements light intensity in media is characterized by applying an empirical relation referred to as Beer's law [49]

$$I = I_o \exp(-\alpha d) \quad \textbf{(3.3)}$$

Here, d is a distance from the surface and α is the absorption coefficient of the material given as [49]

$$\alpha = 4\pi k / \lambda \quad \textbf{(3.4)}$$

Where k is the extinction coefficient and λ is the wavelength.

Figure 3.4 show the absorption coefficients of Al-doped CdO thin films deposited on Si substrate at different growth temperatures. The curves show the maximum peaks from 200 nm to 400 nm, then start decreasing from 400 nm to 1000 nm. The curves show the same behavior of all deposited films. It can also be observed the absorption coefficients of the deposited thin film are also increasing with increase of growth temperature.

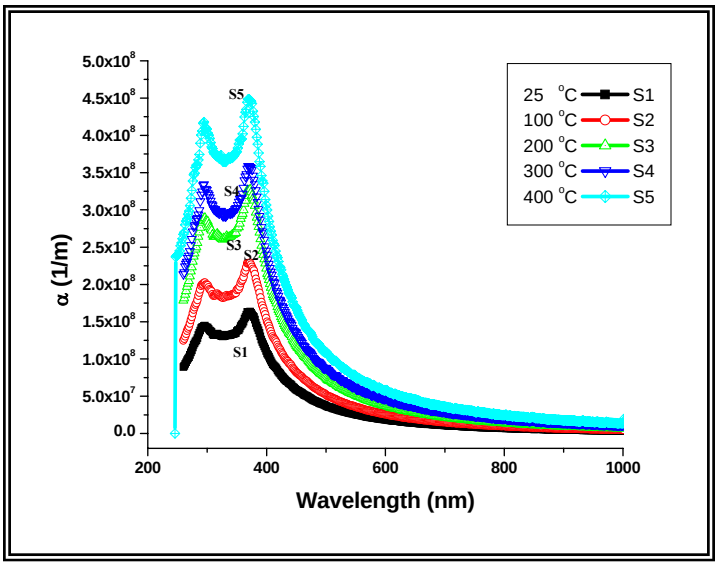

Figure 3.4: Absorption coefficient of Al-doped CdO thin film deposited at different temperature.

The CdO is a material with direct band gap lying in the range: 2.2-2.7 eV [50]. For such band to band transitions the dependence of absorption coefficient α versus photon energy is given by the relation [49].

$$(\alpha h\upsilon)^2 = A\,(h\upsilon - E_g) \qquad \textbf{(3.5)}$$

Where A is a parameter independent of hυ and E_g is the optical band gap energy. Plotting the graph of $(\alpha h\upsilon)^2$ and hυ, the value of E_g can be determined by extrapolating the linear portion of this plot to $(\alpha h\upsilon)^2 = 0$ [51]. By using this method, the optical band gap energy of Al-doped thin films at different growth temperature are found and shown in figure 3.5. Figures show that the optical band gap energy of the deposited thin films is shifted to lower energy when they are deposited at different temperatures. The obtained values of optical band gap energy of Al-doped CdO thin films are from 2.8 eV to 2.6 eV.

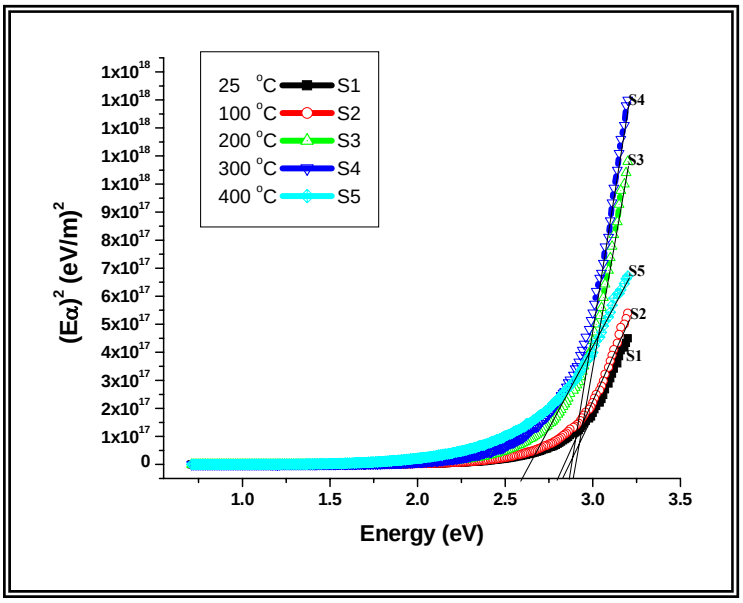

Figure 3.5: Plot of $(\alpha h\upsilon)^2$ versus $h\upsilon$ of Al-doped CdO thin film deposited at different temperature.

Ellipsometry is an optical measurement technique that characterizes light reflection or transmission from samples. We cannot measure optical constants directly from Ellipsometry but change in light polarization expressed as ψ and Δ can be measured by it. The two values (ψ, Δ) represent the amplitude ratio and phase difference between light waves known as p- and s-polarized light waves. These values are related to the ratio of Fresnel reflection coefficients, R_p and R_s for the p and s-polarized light, respectively. [52]

$$\tan \psi \exp (i\Delta) = R_p / R_s \qquad (3.6)$$

In spectroscopic Ellipsometry, (ψ, Δ) spectra of Al-doped CdO deposited thin films at different temperature are measured by changing the wavelength of light as shown in the figure 3.6 All curves show almost same variation in ψ and Δ with respect to wavelength and at different deposition temperature. As ψ is the relative amplitude change related to extinction coefficient, absorption co efficient and band gap energy. Where as Δ is the relative phase change which is related to refractive indices, absorption and reflection of polarized light from material.

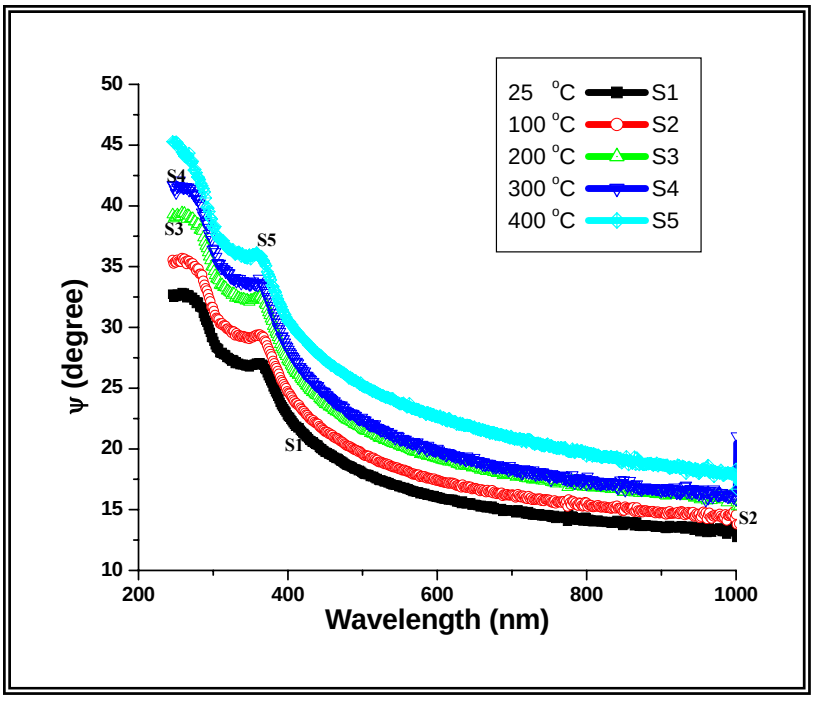

Figure 3.6: SE parameter ψ of Al-doped CdO thin film deposited at different temperature.

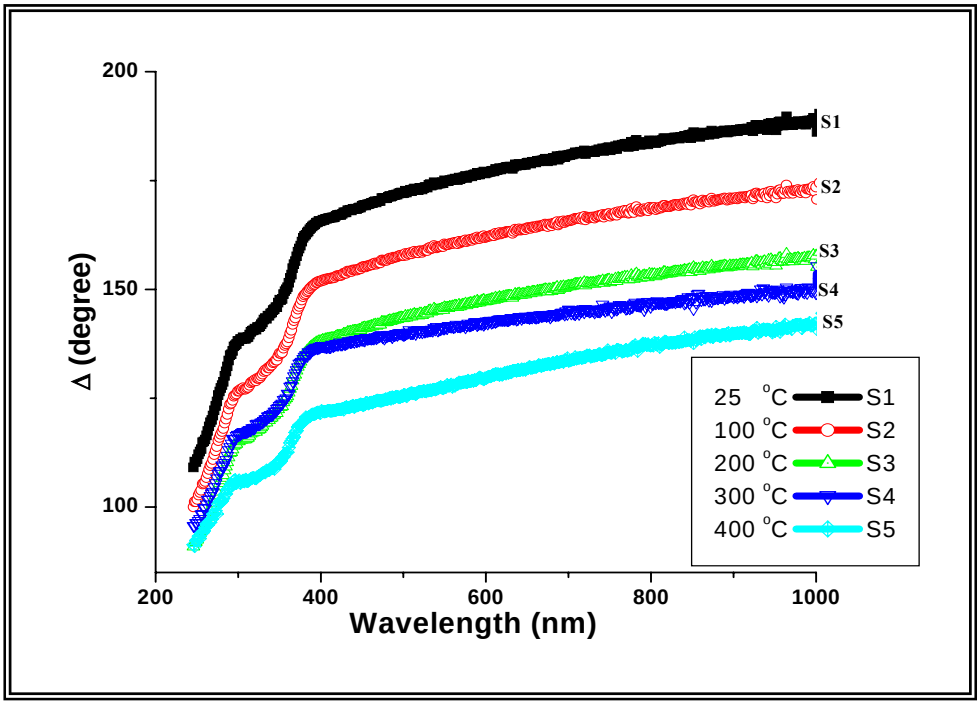

Figure 3.7: SE parameter Δ of Al-doped CdO thin film deposited at different temperature.

When electromagnetic radiation stikes a surface, some is reflected, some absorbed and some transmitted. The reflectivity and aborptivity of thin are calculated by using values of refractive index n, and extinction coefficient k using following relation [53]

$$R = \frac{(n-1)^2 + k^2}{(n+1)^2 + k^2} \quad \textbf{(3.7)}$$

The aborptivity A of an opaque material is [53]

$$A = 1 - R \quad \textbf{(3.8)}$$

$$A = \frac{4n}{(n+1)^2 + k^2} \quad \textbf{(3.9)}$$

The aborptivity and reflectivity of thin films are calculated by using above equations and then plotted calculated values verses wavelength as shown in figures.

Figure 3.8a show Aborptivity A and figure 3.8b show Reflectivity R of Al-doped CdO thin films on Silicon substarte at different temperatures.

From figure 3.8a thin films show maximum reflectivity at shorter wavelengths and it decreases with increase of wavelenght. While maximum absorption at longer wavelengths and decreases as wavelengths decreases. Reflectivity increasing and aborptivity decreasing with increase of growth temperature of all deposited thim films. In UV region reflectivity is maximum but aborptivity in minimun. Where as in vissible and IR regions reflectivity decreases while aborpitivity increases.All reflection curves show maximum refelctivity in IR region, while all aborption curves shows maximum aborptivity in the same region.The increase in absorption and decrease in reflection is due to increase of film thickness and the growth temperature of all deposited thin films.

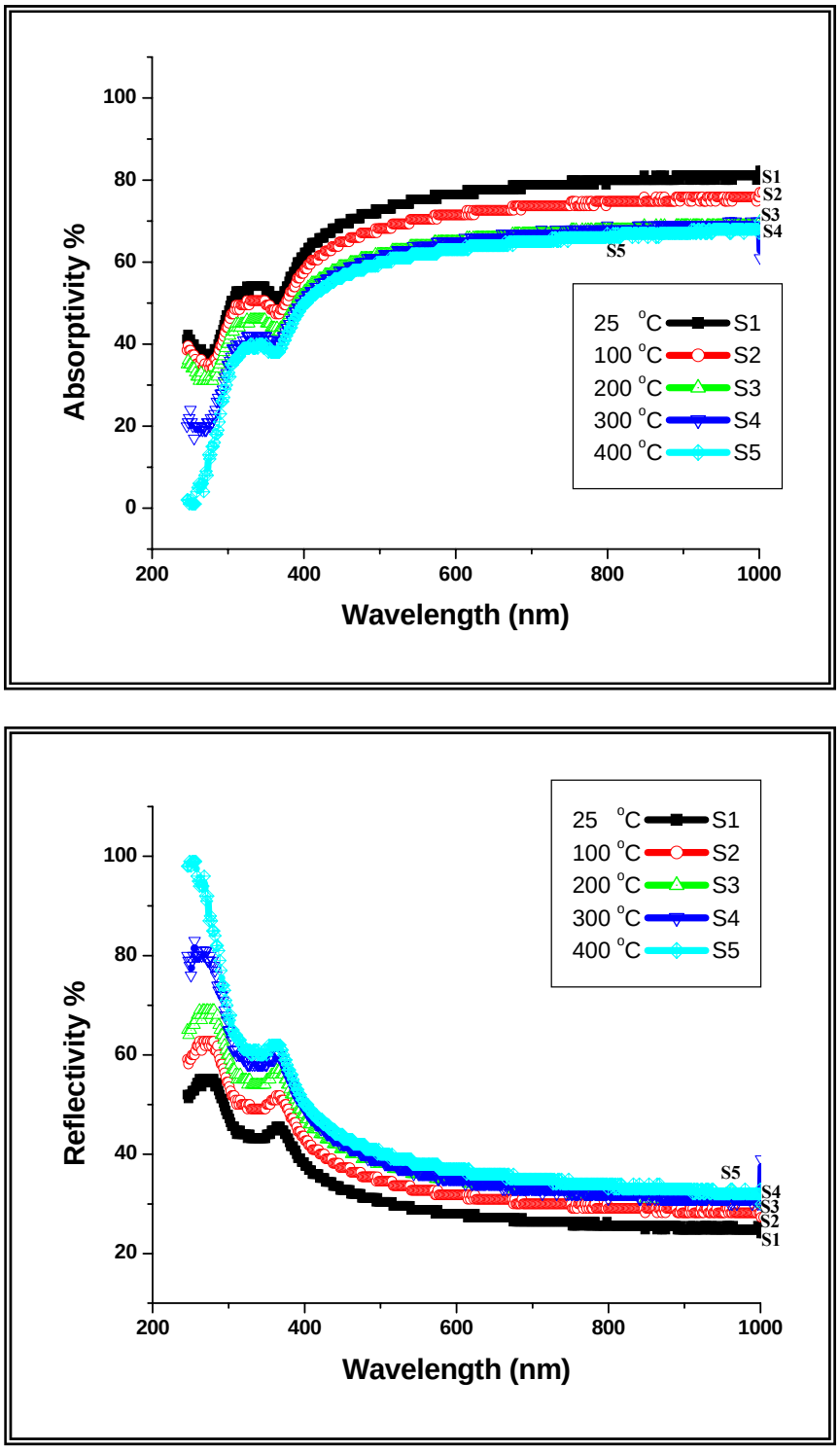

Figure 3.8: Plot of (a) Absorptivity and (b) Reflectivity as a function of wavelength for Al-doped CdO thin film deposited at different temperature.

Free electrons in metals and free carriers in semiconductors absorb light and alter dielectric functions]. The Drude model has been applied widely to describe such light absorption [49]. The complex dielectric constant is define as

$$\varepsilon = \varepsilon_1 - i\varepsilon_2 \quad \textbf{(3.9)}$$

So according to the Drude's theory the real and imaginary parts of the dielectric function can be expressed as [54]

$$\varepsilon_1 = n^2 - k^2 \quad \textbf{(3.10)}$$

$$\varepsilon_2 = 2nk \quad \textbf{(3.11)}$$

Using the above equations the real and the imaginary part of complex dielectric constant of Al-doped CdO deposited films on Silicon substrate at different growth temperature were calculated and plotted in figure (3.9a, 3.9b) as a function of wavelengths.

It can be seen in figure 3.9a that the real dielectric constants are minimum in UV region. Then it starts increasing from visible to IR region. Also due to increase in growth temperature the real part of dielectric constant is also decreasing from shorter wavelengths to the longer ones.

Figure (3.9b) shows the imaginary part of dielectric constant of all deposited thin films at different growth temperatures. All curves show the maximum peak at 380 nm and then they start decreasing as the wavelengths increasing. Also it can be observed that due to increase of growth temperature of the deposited films, it is also increasing.

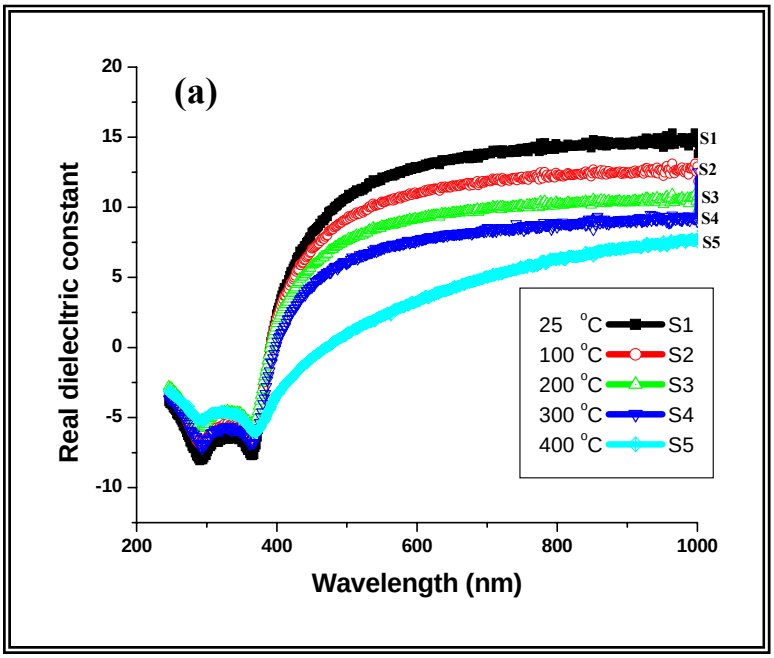

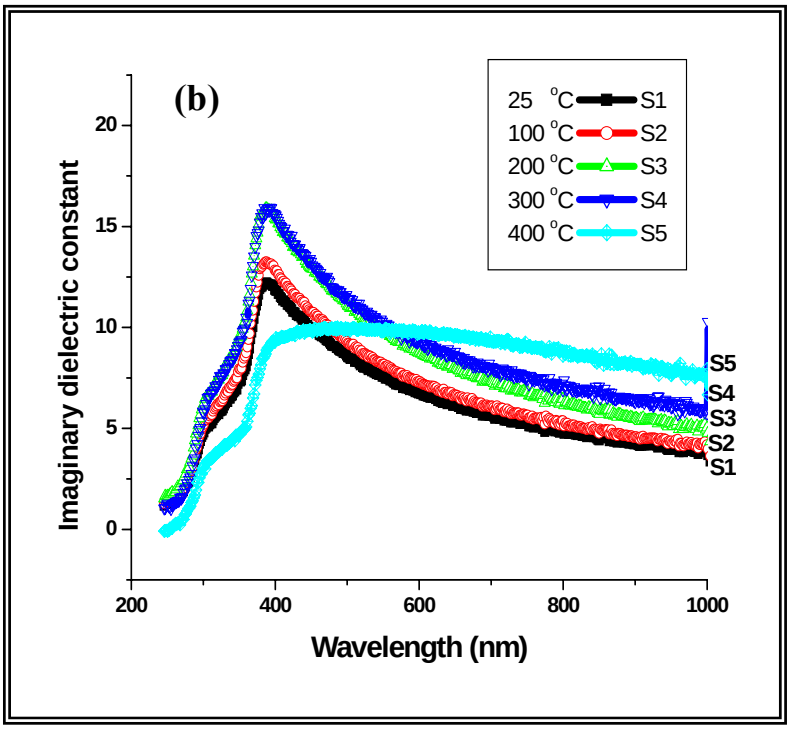

Figure 3.9: Plot of (a) real and (b) imaginary parts of dielectric constants as a function of wavelength for Al-doped CdO thin film deposited at different temperature.

3.3 Magnetometry

Vibrating Sample Magnetometry (Lakeshore 7407) is used to investigate the magnetic properties of Al-doped CdO thin films on Silicon (Si) substrate at different growth temperature. The samples were placed between two magnetic coils and vibrated extremely rapidly. The resulting magnetic moments (M) is measured as a function of applied magnetic filed (H).

The calculated values of saturation magnetization M_s, the Remanence M_r, the coercivity H_c, the squareness ratio SQR of Al-doped CdO thin films deposited on Silicon at different growth temperatures are shown in table 3.2. It is clearly observed from the table that with increase in temperature, Remanence, Coercivity and SQR has been increased. The increase in coercivity shows that at high temperature the material retained its magnetic field more as compare to lower temperature. Hence to demagnetize the material more external field is required which is indicated by increase in Remanence.

Table 3.2: Saturation magnetization M_s, Remanence M_r, Coercivity H_c and Squareness ratio SQR of Al-doped CdO thin film deposited at different temperature.

Sample name	**Deposition temperature °C**	**Saturation magnetization M_s (emu/g) x 10^{-3}**	**Remanence M_r (emu/g)**	**Coercivity H_c (Oe) x 10^2**	**SQR = (M_r/ M_s) x 10^3**
S1	25	1.07	1.966	2.40	1.837
S2	100	1.07	5.290	3.12	4.943
S3	200	1.07	6.345	3.54	5.929
S4	300	1.07	7.137	3.84	6.670
S5	400	1.07	8.534	4.54	7.975

The values are also plotted in figure 3.10. Figure 3.10a shows that Remanence M_r, mean magnetization left behind in the material after an external magnetic field is removed, of the deposited thin films on silicon substrate is temperature depended. The Remanence of the deposited material is increasing with increase of growth temperature.

Figure 3.10b shows the Coercivity H_c of the same material. This also described the same behavior. In figure 3.10c Squareness ratio SQR of Al-doped CdO thin films is plotted against different growth temperatures. They are also increasing with increase of deposition temperature.

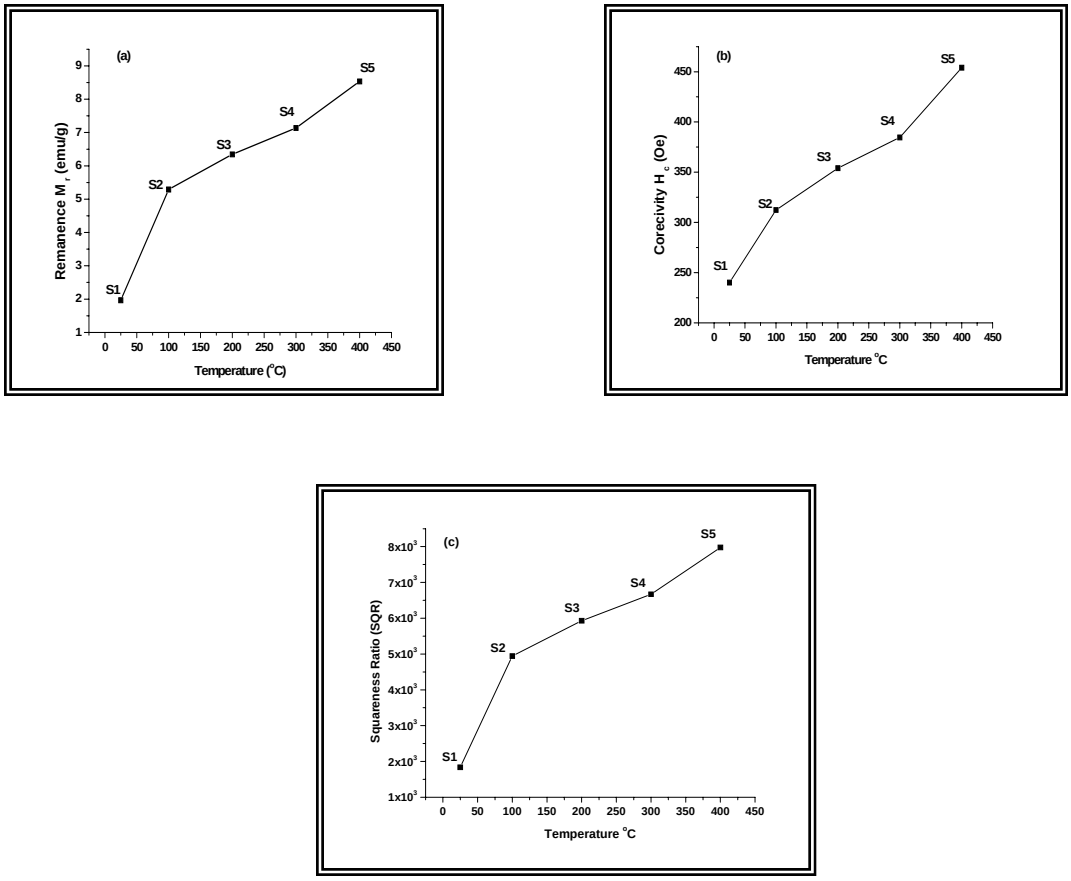

Figure 3.10: Plot of (a) Remanence M_r, (b) Coercivity H_c and (c) Squareness ratio SQR of Al-doped CdO thin film deposited at different temperature.

The magnetization loop of Al-doped CdO thin films on silicon substrate are also plotted in figure 3.11. Figure 3.11a, b, c, d and e shows the M-H loops of the deposited thin film at room temperature, 100 °C, 200°C, 300 °C and at 400 °C respectively. It is clear from the figures that area of hysteresis loop of the deposited thin films is increasing with increase of the growth temperature. This shows that at higher temperature it is more difficult to magnetize or demagnetize material hence the behavior of the material is shifting from soft magnetic material to hard magnetic material.

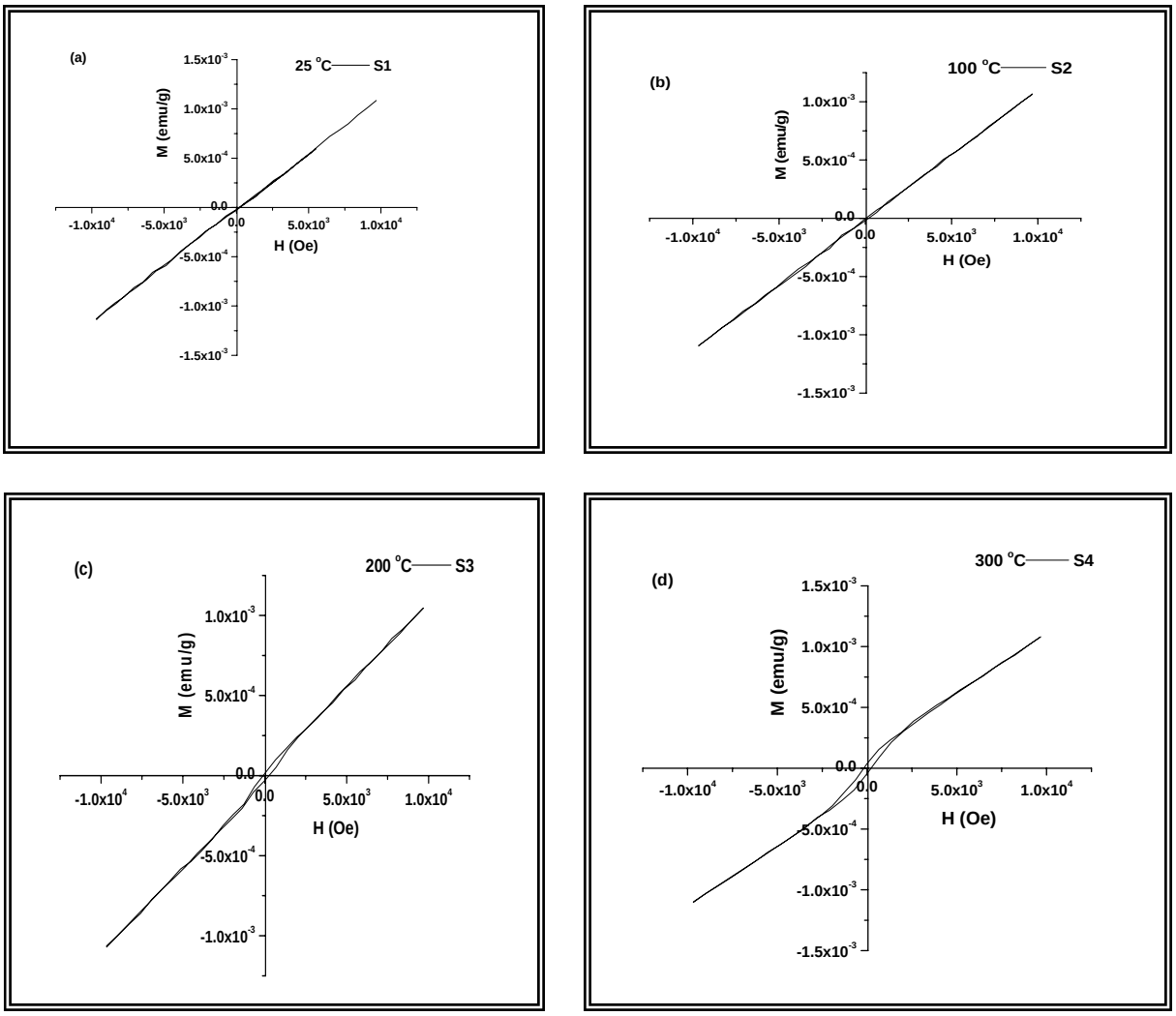

Figure 3.11: Magnetization loop of Al-doped CdO thin films at (a) 25 °C (b) 100 °C and (c) 200 °C (d) 300 °C

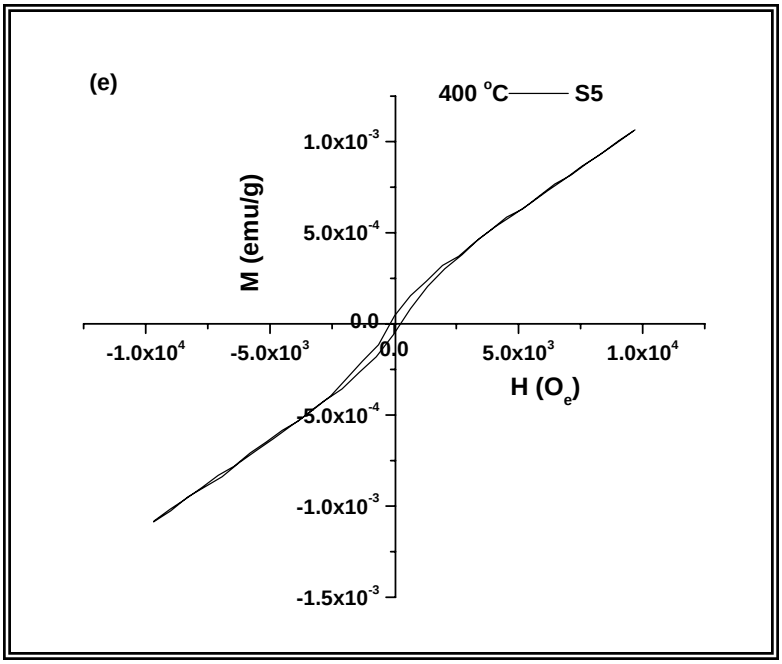

Figure 3.12: Magnetization loop of Al-doped CdO thin films at (e) 400 °C

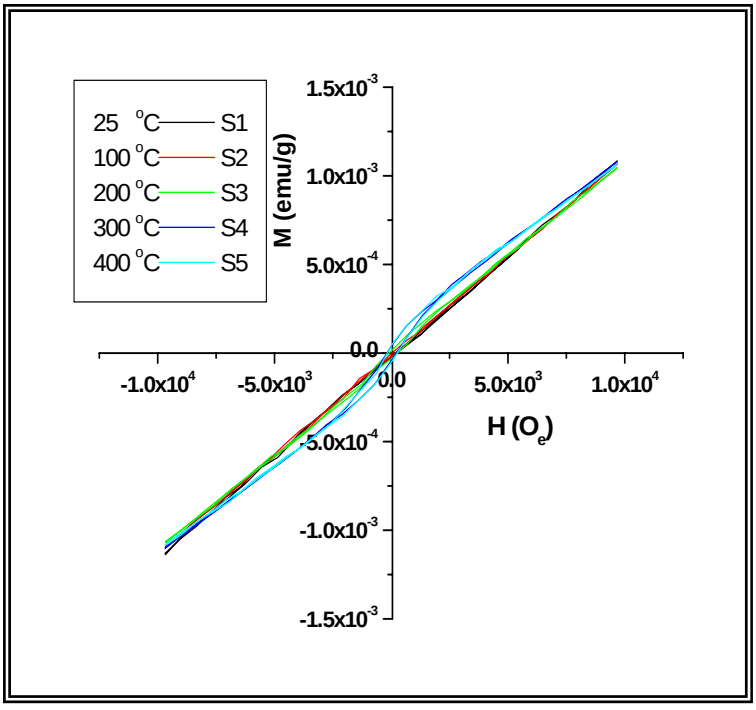

Figure 3.13: Combined Plot of M-H loops of Al-doped CdO thin film deposited at different temperature.

3.4 SEM Analysis of thin film

The morphological microstructure of the deposited Al-doped CdO thin films with the increase of the substrate temperature were studied by SEM (Hitachi 3400N) is shown in figure 3.14. In collaboration with X-ray diffraction patterns, SEM surface images showing morphology-temperature dependence. At room temperature, although amorphous structure is predominant, some microcrystalline aggregates embedded in the non-crystalline matrix appeared. It is clear from the figure that the film surface is rough enough to show non uniform deposition with crater formation, reposition of material and due to different ablation and sputtering mechanisms droplets and flakes of the vaporized target. Non uniform of the thin film may be due to room temperature. Growth of thin film greatly depends upon many factors, such as density, ionization degree and the type of the condensing particles, as well as the temperature and physicochemical properties of the substrate. With increasing the substrate temperature to 200 °C, the deposited films start to show some polycrystalline grains. Further increase of deposition temperature, resulted in more crystallization of the obtained films with rough surfaces [55].

At low substrate temperature, the sputter particles absorbed on the surface of the substrates and shortly move to settle in its lower energy. But at high substrate temperature, the atoms get more energy from the substrate then move longer with more diffusion on the surface. Uniform surface with dense microstructure can be seen for the films deposited at high deposition temperature. Which cold be due to an enlargement of the grains and indicating improvement of the crystal quality with increasing temperature. It is known that the films deposited in vacuum at lower substrate temperatures have very small particle sizes while those deposited at higher substrate temperature have larger grain sizes [56].

The creation of microscopic particles on the surface of thin films deposited by PLD is an undesirable and almost inevitable feature of this process. These particles may also be produced as a result of changes in the surface morphology of the target, roughening of target surface, fracture of the target during laser irradiation. Many mechanisms like surface boiling, exfoliation, hydrodynamic sputtering and splashing may be involved in particulate generation [57].

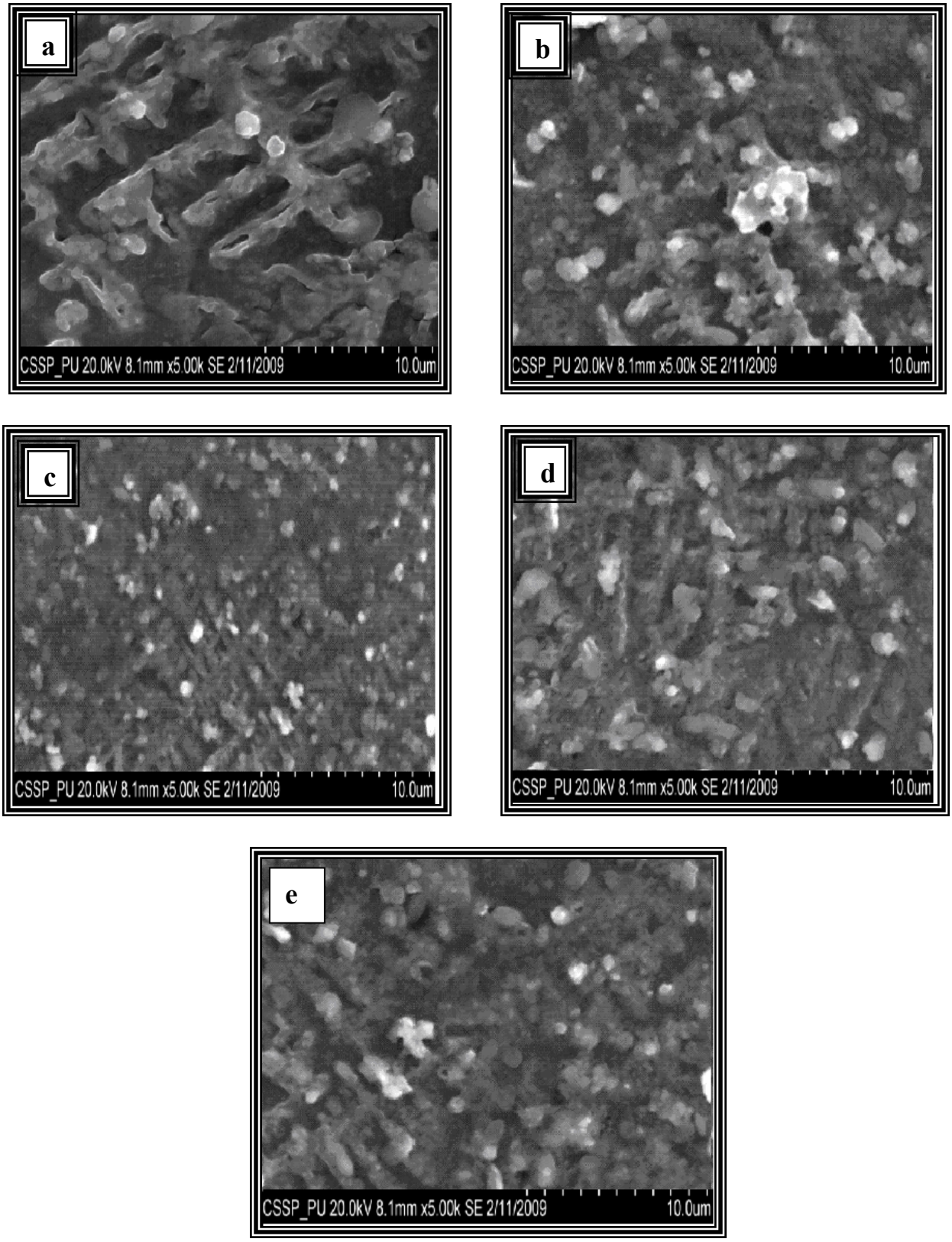

Figure 3.14: SEM images of Al-doped CdO thin films on Silicon substrate at (a) 25 °C (b) 100°C (c) 200°C (d) 300°C (e) 400°C

Chapter 4
CONCLUSION AND FUTURE WORK

4.1 Conclusion

In this research work, Al-doped CdO thin films were deposited by PLD technique on Silicon (111) substrate. The effects of deposition temperature on structural, optical, magnetic properties were studied. The morphology-temperature dependence was also studied by SEM.

The XRD patterns show that deposition temperature affects the preferential growth of the films. The film deposited on unheated substrate was mostly amorphous have both (111) and (200) orientations. While the films grown at high temperature show preferential growth along the (200) direction. It indicates the polycrystalline nature of the CdO with cubic structure. The grain size of the deposited thin film is also increasing with increase of temperature.

The Spectroscopic Ellipsometry graphs show the temperature effect on optical properties of deposited thin films. It has been observed that optical properties vary with growth temperature. The Absorpitivity of the deposited films is decreasing and reflectivity is increasing with the increase of growth temperature. The optical band gap energy of Al-doped CdO thin film is also decreasing with the increase of growth temperature.

The deposition temperatures also show some effect on magnetic properties of the deposited films. The magnetic behavior of the deposited material is increasing with increase of growth temperature. At room temperature the Remanence M_r is minimum, which is increasing with increase of temperature. This indicates that to demagnetize the material more external field is required.

SEM analysis indicates morphological micrographs of the deposited Al-doped CdO thin films with the increase of the substrate temperature. At room temperature, although amorphous structure is predominant, some microcrystalline aggregates embedded in the non-crystalline matrix appeared. With increasing the substrate temperature up to 200 °C, the deposited films start to show some polycrystalline grains. Further increase of deposition temperature, resulted in more crystallization of the obtained films with rough surfaces.

4.2 Future work

Transparent conducting metal oxides thin films are extensively used for different optoelectronics applications. So in future it can be used as

- Transparent electrodes
- Transparent heating elements
- Transparent heat reflecting windows
- Antireflection coating
- Solar cells
- Phototransistors
- Liquid crystal display
- Optical heater
- Gas sensors.

References

[1] O. Svelto, Principles of Lasers (Plenum Press, New York, 1998).

[2] M. von Allmen and A. Blatter, Laser-Beam Interactions with Materials (Springer, Berlin, 1995).

[3] J. C. Miller (editor), Laser Ablation – Principles and Applications (Springer,Berlin, 1994).

[4] D. B. Chrisey and G. K. Hubler (editors), Pulsed Laser Deposition of Thin Films (Wiley, New York, 1994).

[5] M. N. R. Ashfold, F. Claeyssens, G. M. Fuge, and S. J. Henley, Chemical Society Review **33**, 23–31 (2004).

[6] A. Hakola, Large-Area Deposition of High-Temperature Superconducting Thin Films Using Laser Ablation, Master's Thesis (Helsinki University of Technology, 2001).

[7] T. E. Itina, J. Hermann, Ph. Delaporte, and M. Sentis, Thin Solid Films **453–454**, 513–517 (2004).

[8] B. N. Chichkov, C. Momma, S. Nolte, F. von Alvensleben, and A. Tünnermann, Applied Physics Letter **A 63**, 109–115 (1996).

[9] R. F. Haglund Jr., Applied Surface Science **96–98**, 1–13 (1996).

[10] J. N. Leboeuf, K. R. Chen, J. M. Donato, D. B. Geohegan, C. L. Liu, A. A. Puretzky, and R. F. Wood, Applied Surface Science **96–98**, 14–23 (1996).

[11] R. F. Haglund Jr. and N. Itoh, "Electronic processes in laser ablation of semiconductors and insulators" in Laser Ablation – Principles and Applications, J. C. Miller (editor), (Springer, Berlin, 1994).

[12] L. M. Doeswijk, G. Rijnders, and D. H. A. Blank, Applied Physics Letter **A 78**, 263–268 (2004).

[13] B. Toftmann, J. Schou, T. N. Hansen, and J. G. Lunney, Applied Surface Science **186**, 293–297 (2002).

[14] B. Toftmann, J. Schou, T. N. Hansen, and J. G. Lunney, Physical Review Letters **84**, 3998–4001 (2000).

[15] S. Amoruso, B. Toftmann, and J. Schou, Physical Review Letters **E 69**, 056403-1–6 (2004).

[16] W.-F. Hu, X.-J. Zhao,W. Peng, T.-S.Wang,W. Liu, L. Li, C. Lei, Y.-F. Chen, and L. Li, Journal of Crystal Growth **231**, 493–497 (2001).

[17] D. H. A. Blank, G. Koster, G. A. J. H. M. Rijnders, E. van Setten, P. Slycke, and H. Rogalla, Journal of Crystal Growth **211**, 98–105 (2000).

[18] B. Dam, J. H. Rector, J. M. Huijbregtse, and R. Griessen, Physica **C 305**, 1–10 (1998).

[19] D. Q. Shi, M. Ionescu, T. M. Silver, and S. X. Dou, Physica **C 384**, 475–481 (2003).

[20] S. Kahl and A. M. Grishin, Journal of Applied Physics **93**, 6945–6947 (2003).

[21] A. Klini, A. Manousaki, D. Anglos, and C. Fotakis, Journal of Applied Physics **98**, 123301-1–8 (2005).

[22] R.K. Gupta, K. Ghosh, R. Patel, S.R. Mishra, P.K. Kahol, Applied Surface Science **254** 5868–5873 (2008).

[23] R.K. Gupta, K. Ghosh, R. Patel, S.R. Mishra, P.K. Kahol, Materials Letters **62** 4103- 4105 (2008).

[24] R.K. Gupta, K. Ghosh, R. Patel, S.R. Mishra, P.K. Kahol, Materials Letters **62** 3373–3375 (2008).

[25] B. Saha, S. Das, K.K. Chattopadhyay, Solar Energy Materials & Solar Cells **91** 1692–1697 (2007).

[26] J. Santos-Cruz, G. Torres-Delgado, R. Castanedo-Perez, S. Jime´nez-Sandoval O. Jime´nez-Sandoval, C.I. Zu´n˜iga-Romero, J. Ma´rquez Marı´n, O. Zelaya-Angel, Thin Solid Films **493** 83 – 87 (2005).

[27] W. Miao, X. Li, Q. Zhang, L. Huang, Z. Zhang, L. Zhang, X. Yan, Thin Solid Films **500** 70 – 73 (2006).

[28] R. Mamazza Jr., D. L. Morel, C. S. Ferekides, Thin Solid Films **484** 26 – 33 (2005).

[29] W. Beyer, J. Hüpkes , H. Stiebig, Thin Solid Films **516** 147–154 (2007).

[30] R. Maity, K.K. Chattopadhyay, Solar Energy Materials & Solar Cells **90** 597–606 (2006).

[31] I. Saadeddin, B. Pecquenard, J.P. Manaud, R. Decourt, C. Labruge`re T. Buffeteau, G. Campet, Applied Surface Science **253** 5240–5249 (2007).

[32] S. Moo Park, T. Ikegami, K. Ebihara, P. Kyun Shin, Applied Surface Science **253** 1522–1527 (2006).

[33] C.H. Bhosale, A.V. Kambale, A.V. Kokate, K.Y. Rajpure, Materials Science and Engineering **B 122** 67–71(2005).

[34] R.K. Gupta, K. Ghosh, S.R. Mishra, P.K. Kahol, Applied Surface Science **254** 4018– 4023 (2008).

[35] L. Zhao, J. Lian, Y. Liu, Q. Jiang, Applied Surface Science **252** 8451– 8455 (2006).

[36] D. Kim, E. Byon, G. H. Lee, S. Cho, Thin Solid Films **510** 148–153 (2006).

[37] L.R. de León-Gutiérrez, J.J. Cayente-Romero, J.M. Peza-Tapia, E. Barrera-Calva J.C. Martínez-Flores, M. Ortega-López, Materials Letters **60** 3866–3870 (2006).

[38] T.K. Yong, T.Y. Tou, B.S. Teo, Applied Surface Science **248** 388–391 (2005).

[39] W. Wohlmutha, I. Adesida, Thin Solid Films **479** 223– 231 (2005).

[40] E.J.J. Martin, M. Yan, M. Lane, J. Ireland, C.R. Kannewurf, R.P.H. Chang, Thin Solid Films **461** 309– 315(2004).

[41] W. T. Silfvast, Laser Fundamentals 2nd edition (Cambridge University Press 2004) pp 516-520.

[42] R. M. Besançon. V. N. Reinhold "Vacuum Techniques". The Encyclopedia of Physics (3rd edition), New York,(1990) . 1278-1284.

[43] www.en.wikipedia.org

[44] M. F. A. M. V. Hest, Ph.D. thesis, High Rate Plasma Deposition of Silicon Oxide Like Films, Department of Applied Physics, Center for Plasma Physics and Radiation Technology, Eindhoven University of Technology, Netherlands (2002).

[45] K. H. J. Buschow and F. R. deBoer, Physics of magnetism and magnetic materials (Kluwer Academic Publishers New York, 2004) pp 87.

[46] V.I. Anisimov, I.S. Elfimov, N. Hamada, K. Terakura, Physical Review B 54, 4387-4390 (1996)., M. Mottaa, C.V. Deimlingb, W.A. Ortizb, P.N. Lisboa-Filhoa, Journal of Magnetism and Magnetic Materials 320, 496–499 (2008)**.**

[47] B. D. Culity, Elements of X-ray diffraction 2nd edition Addison Wesley Publishing Company, inc, London, 1978).

[48] F. I. Ezema, P.U. Asogowa, A. B. C. Ekwealor, P.E. Ugwuoke, R.U. Osuji, Journal of the University of chemical Technology and Metallurgy, **42**, 217-222, (2007).

[49] H. Fujiwara, Spectroscopic Ellipsometry principles and applications Japanese edition (John Wiley & Sons Ltd, England 2007) pp 22-23.

[50] K. L Chopra, S. R. Das, Thin Films Solar Cells, Plenum Press, New York (1993).

[51] R. S. Rusu, G. I. Rusu, Journal of Optoelectronics and Advance Materials **70**, 823-828 (2005).

[52] H. Fujiwara, Spectroscopic Ellipsometry principles and applications Japanese edition (John Wiley & Sons Ltd, England 2007) pp 82.

[53] M. Ohning, The material science of thin films United Kingdom Edition (Academic Press Limited, 1992) pp 510.

[54] H. A.Hafez Mohammed and H. M. Ali, Science and Technology of Advance Materials **9,** 025016 9pp (2008).

[55] E. M. EI-Maghraby. Journal of Crystal Research and Technology **43**, 9,970-974 (2008).

[56] Y. E. Yee, J. B. Lee, Y. J. Kim, H. K. Yang, J. C. Park and H. J. Kim. Journal of Vacuum Science and Technology. A **14** 1943 (1996).

[57] P. G. Kotula, C.B. Carter, M. G. Norton. Journal of Materials Science Letters **13**, 1275-1277 (1994).